Supplementary Information

Photonic Control of Thermal Radiation for Protective Windows

YUNBIN YING,[1] JIANBO YU,[1] WEIDONG SHEN,[1] PINTU GHOSH,[1,*] MIN QIU,[2] AND QIANG LI[1,*]

[1]*State Key Laboratory of Modern Optical Instrumentation, College of Optical Science and Engineering, Zhejiang University, Hangzhou 310027, China*
[2]*Key Laboratory of 3D Micro/Nano Fabrication and Characterization of Zhejiang Province, School of Engineering, Westlake University, Hangzhou 310024, China*

*qiangli@zju.edu.cn；*ghosh@zju.edu.cn*

Section 1. Theoretical model of directional radiative cooling

As shown in Fig. 1d, we consider a directional radiative cooler of area A at temperature T_{Sam} facing a high-temperature thermal source ($T_{Sou} > 700\mathrm{K}$). When the directional thermal emitter is exposed under non-uniform environmental conditions, it is subject to both emissions from the high-temperature thermal source at temperature and atmospheric thermal radiation (corresponding to ambient air temperature T_{Amb}). The steady-state condition is given by:

$$P_{rad}\left(T_{Sam}\right)+P_{cond+conv}=P_{heating}\left(T_{Sou}\right)+P_{Atm}\left(T_{Amb}\right) \tag{S1}$$

The temperature of the directional thermal emitter can be calculated according to the above equation when the system is in a steady state.

For further analysis of steady-state conditions, we defined half-view angle (α) as the collection half-angle, which is decided by the size of the external thermal source and the distance between the sample and the thermal source. And, the directional emission angle (θ_e) is decided by the directional thermal emitter as shown in Fig. S1. The power radiated out by the sample can be considered in two cases:

$$P_{rad}\left(T_{Sam}\right)=\begin{cases} A2\pi\int_{\theta_e}^{\pi/2}\mathrm{d}\theta\sin\theta\cos\theta\int_0^{\infty}\mathrm{d}\lambda I_{BB}\left(T_{Sam},\lambda\right)\varepsilon\left(\lambda,\theta\right) & \alpha\le\theta_e \\ A2\pi\int_{\alpha}^{\pi/2}\mathrm{d}\theta\sin\theta\cos\theta\int_0^{\infty}\mathrm{d}\lambda I_{BB}\left(T_{Sam},\lambda\right)\varepsilon\left(\lambda,\theta\right) & \alpha>\theta_e \end{cases} \tag{S2}$$

Here, I_{BB} is the spectral radiance of a blackbody. $\varepsilon\left(\lambda,\theta\right)$ is the spectral and angular emissivity of the directional thermal emitter (DTE) as shown in Fig. S1.

$$P_{cond+conv}=Ah_c\left(T_{Sam}-T_{Amb}\right) \tag{S3}$$

Here, $P_{cond+conv}$ is the power lost due to convection and conduction. h_c is a comprehensive non-radiative heat coefficient that captures the collective effect of conductive and convective heating.

The temperature of the thermal source is much higher than that of the sample, while the size of the sample is much smaller than that of the thermal source, hence the sample absorbs a substantial amount of thermal radiation and subsequent heating when exposed to high-temperature heat sources. The heating emission power from the external high-temperature thermal source is approximately:

$$P_{heating}\left(T_{Sou}\right)\approx\begin{cases} 0 & \alpha\le\theta_e \\ A2\pi\int_{\theta_e}^{\alpha}\mathrm{d}\theta\sin\theta\cos\theta\int_0^{\infty}\mathrm{d}\lambda I_{BB}\left(T_{Sou},\lambda\right)\varepsilon_{Sou}\left(\lambda,\theta\right) & \alpha>\theta_e \end{cases} \tag{S4}$$

Here, $\varepsilon_{Sou}\left(\lambda,\theta\right)$ is the spectral and angular emissivity of the thermal source that can be seen as an ideal blackbody as shown in Fig. S1.

T_{Sou} is set to 700 K. T_{Amb} is set to 320 K. h_c is set to 20 $\mathrm{Wm^{-2}K^{-1}}$. Hence, the steady-state temperature (T_{Sam}) of the directional thermal emitter varying with the half-view angle (α) and the directional emission angle (θ_e) can be calculated according to the above equations as shown in Fig. S2. The half-view angle is from 20°to 60° at 5° increments, and the directional emission angle is from 0°to 90°at 5° increments.

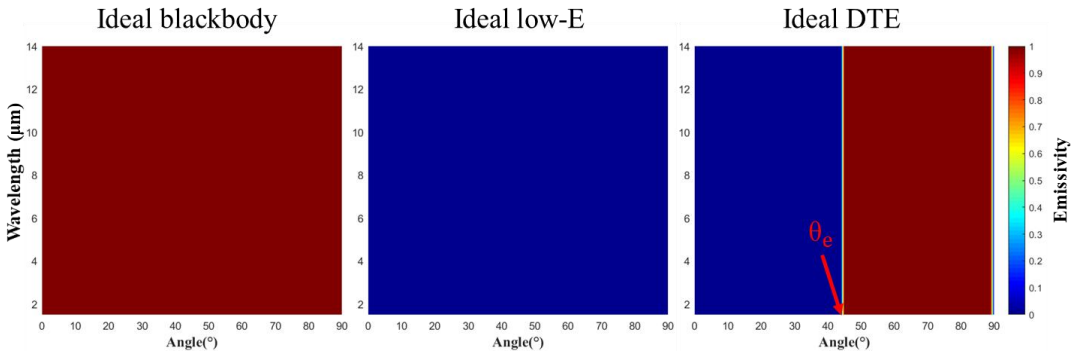

Fig. S1. The emissivity spectrum varying with the angle for an ideal blackbody (left), ideal low-E (middle), and ideal DTE (right).

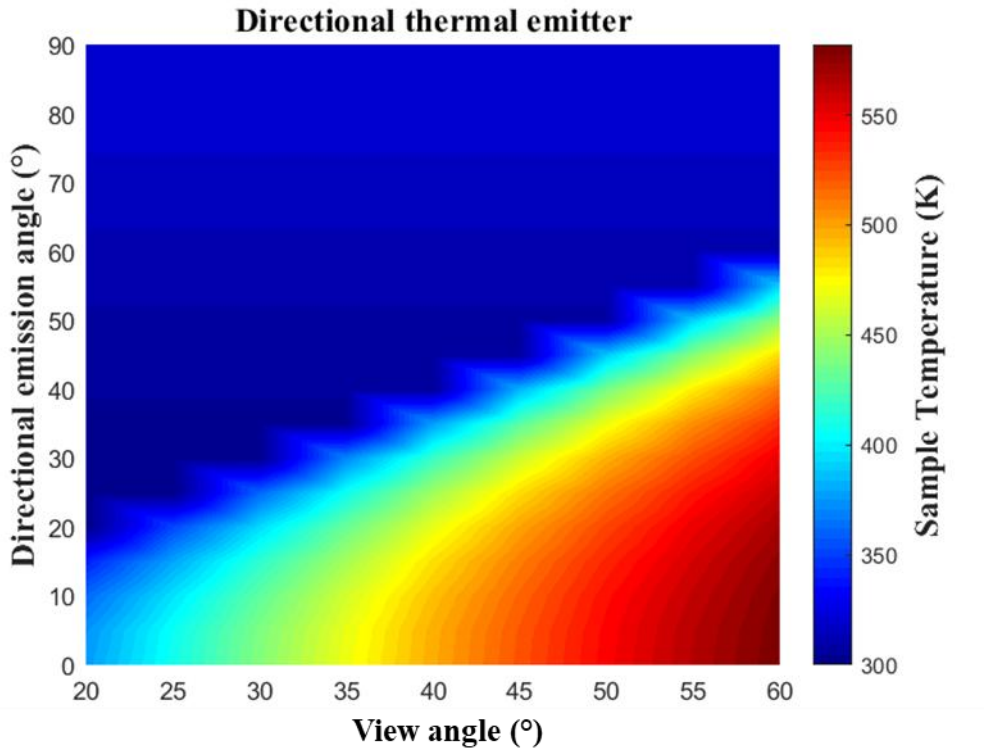

Fig. S2. A map of the calculated steady-state sample temperature (T_{Sam}) as a function of the half-view angle (α) and the directional emission angle (θ_e).

Section 2. Simulated and measured results

Numerical reflection spectra and emissivity spectra were generated using a radio frequency module (electromagnetic waves, frequency domain) in the commercially available COMSOL Multiphysics. The simulation was performed using a 2D model with incident plane wave. Periodic boundary conditions were used in the x-direction and perfectly matched layers were used in the y-direction (normal to the sample). The refractive index and extinction coefficient of polycarbonate (PC), Al_2O_3, and ZnS were obtained from Ref. [1-3], respectively. According to Kirchhoff's law of thermal radiation, the simulated emissivity can be replaced by the simulated absorptivity, and the emission angles can be replaced by the incident angles.

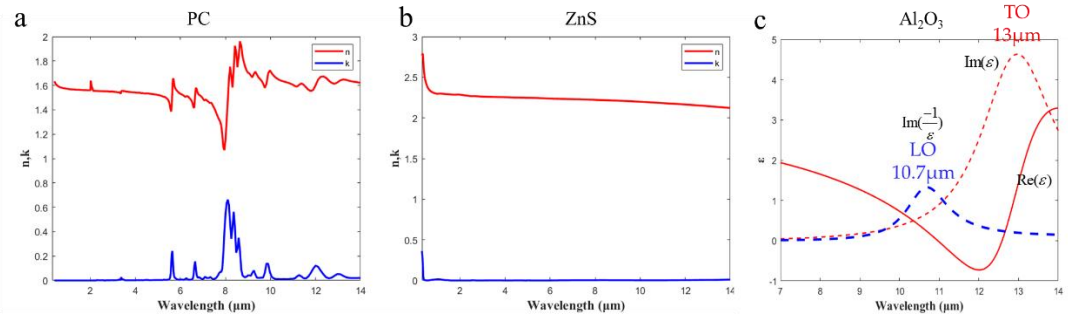

Fig. S3. (a) The refractive index and extinction coefficient of the PC. **(b)** The refractive index and extinction coefficient of the ZnS. **(c)** The permittivity of the Al_2O_3. The wavelength of the longitudinal optical phonon polariton (LO) is about 10.7 μm, the wavelength of transverse optical phonon polariton (TO) is about 13 μm.

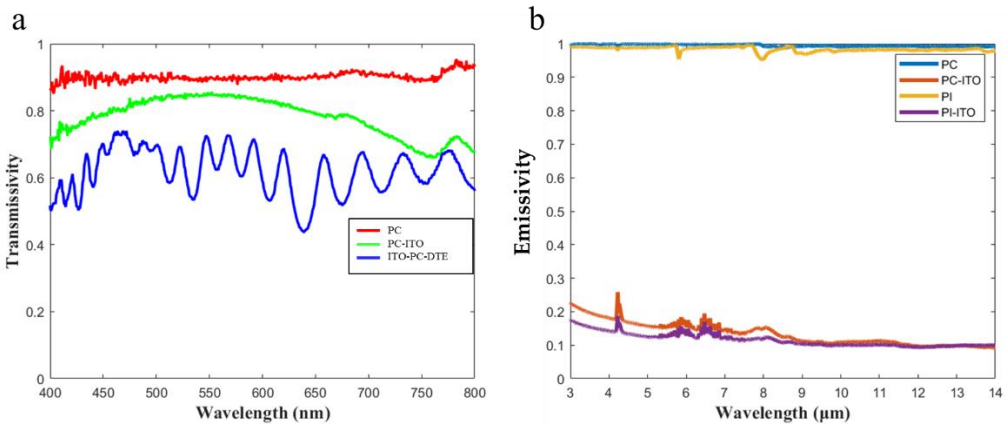

Fig. S4. (a) The measured visible transmissivity of PC, PC-ITO, and ITO-PC-DTE. **(b)** The measured infrared emissivity of PC, PC-ITO, PI, and PI-ITO.

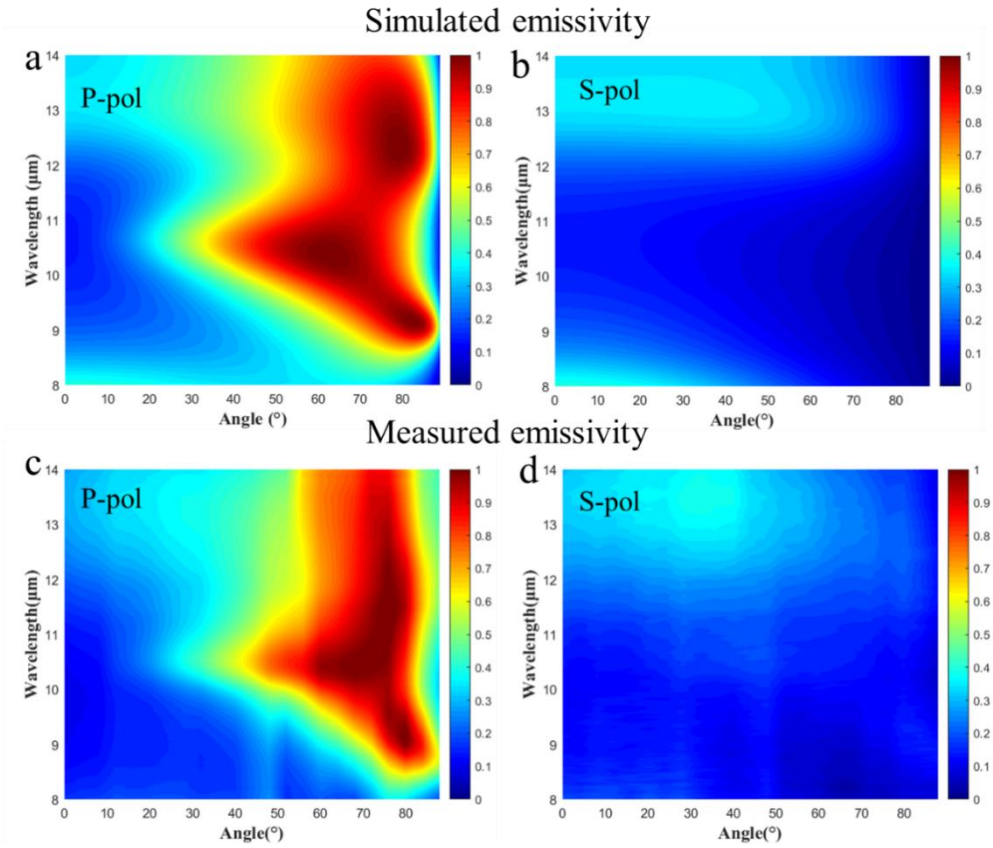

Fig. S5. Experimental characterization and simulation of nanophotonic-engineered thermal protective window. (a) and (b) The simulated emissivity spectrum in p-polarization and s-polarization varying with angle for the NETPW. (c) and (d) The measured emissivity spectrum in p-polarization and s-polarization varying with angle for the NETPW.

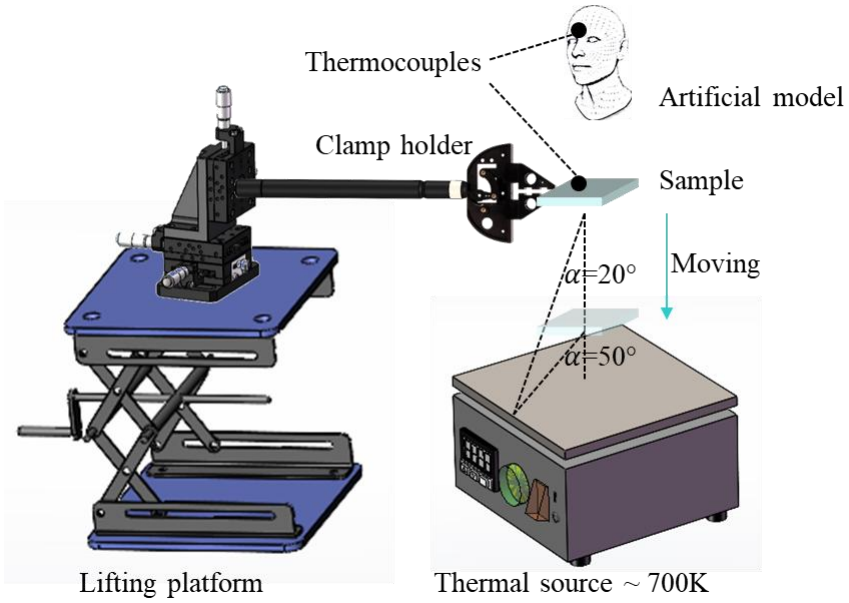

Fig. S6. Schematic of the experimental setup to demonstrate the thermal protection and thermal comfort performance.

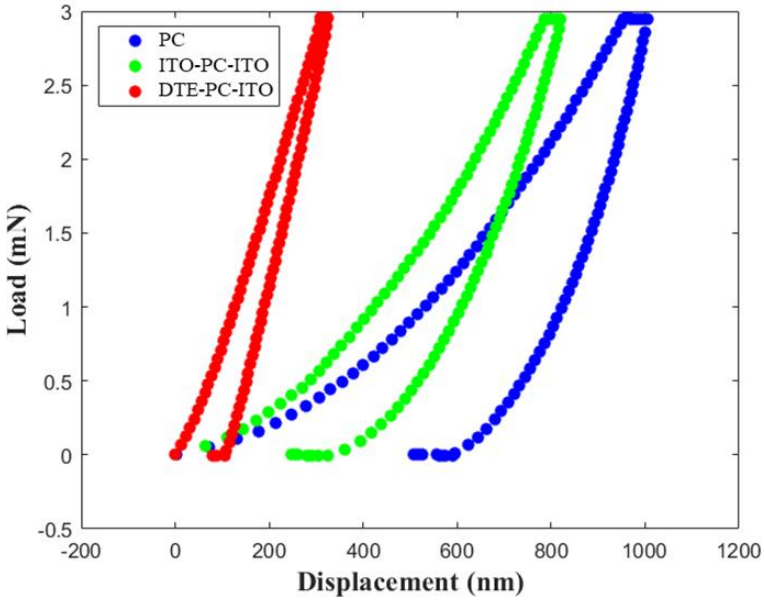

Fig. S7. Load-displacement curves of PC, ITO-PC-ITO, DTE-PC-ITO.

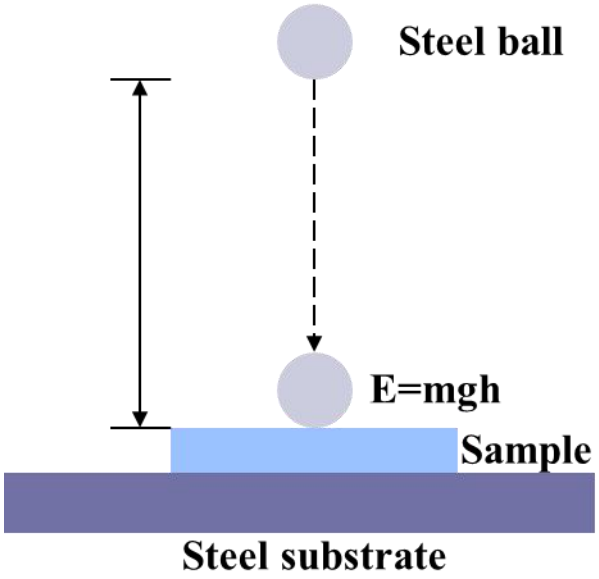

Fig. S8. Schematic of the falling ball impact test to demonstrate the impact resistance performance.

References

1. Kischkat, J. et al., Mid-infrared optical properties of thin films of aluminum oxide, titanium dioxide, silicon dioxide, aluminum nitride, and silicon nitride. *Applied Optics* **51**, 6789 (2012).
2. Sultanova, N. et al. Dispersion properties of optical polymers. *Acta Physica Polonica A* **116**, 585 (2009).
3. Zhu, H. et al., Multispectral camouflage for infrared, visible, lasers and microwave with radiative cooling. *Nature Communications* **12**, 1805 (2021).